Brian Davis
Department of Mechanical and Aerospace Engineering, University of Florida, Gainesville, FL 32611

David Dabrow
Department of Mechanical and Aerospace Engineering, University of Florida, Gainesville, FL 32611

Ryan Newell
Department of Materials Science and Engineering, University of Central Florida, Orlando, FL 32816

Andrew Miller
Department of Mechanical and Aerospace Engineering, University of Florida, Gainesville, FL 32611

John K. Schueller
Department of Mechanical and Aerospace Engineering, University of Florida, Gainesville, FL 32611

Guoxian Xiao
General Motors Global R&D, Warren, MI 48090

Steven Y. Liang
George W. Woodruff School of Mechanical Engineering, Georgia Institute of Technology, Atlanta, GA 30332

Karl T. Hartwig
Materials Science and Engineering Department, Texas A&M University, College Station, TX 77843-3003

Nancy J. Ruzycki
Department of Material Science and Engineering, University of Florida, Gainesville, FL 32611

Yongho Sohn
Department of Materials Science and Engineering, University of Central Florida, Orlando, FL 32816

Yong Huang[1]
Department of Mechanical and Aerospace Engineering, University of Florida, Gainesville, FL 32611; Department of Material Science and Engineering, University of Florida, Gainesville, FL 32611
e-mail: yongh@ufl.edu

Chip Morphology and Chip Formation Mechanisms During Machining of ECAE-Processed Titanium

Severe plastic deformation (SPD) processing such as equal channel angular extrusion (ECAE) has been pioneered to produce ultrafine grained (UFG) metals for improved mechanical and physical properties. However, understanding the machining of SPD-processed metals is still limited. This study aims to investigate the differences in chip morphology when machining ECAE-processed UFG and coarse-grained (CG) titanium (Ti) and understand the chip formation mechanism using metallographic analysis, digital imaging correlation (DIC), and nano-indentation. The chip morphology is classified as aperiodic saw-tooth, continuous, or periodic saw-tooth, and changes with the cutting speed. The chip formation mechanism of the ECAE-processed Ti transitions from cyclic shear localization within the low cutting speed regime (such as 0.1 m/s or higher) to uniform shear localization within the moderately high cutting speed regime (such as from 0.5 to 1.0 m/s) and to cyclic shear localization (1.0 m/s). The shear band spacing increases with the cutting speed and is always lower than that of the CG counterpart. If the shear strain rate distribution contains a shift in the chip flow direction, the chip morphology appears saw-tooth, and cyclic shear localization is the chip formation mechanism. If no such shift occurs, the chip formation is considered continuous, and uniform shear localization is the chip formation mechanism. Hardness measurements show that cyclic shear localization is the chip formation mechanism when localized hardness peaks occur, whereas uniform shear localization is operative when the hardness is relatively constant.
[DOI: 10.1115/1.4038442]

Keywords: equal channel angular extrusion, titanium, machining, chip formation, chip morphology

[1]Corresponding author.
Manuscript received June 3, 2017; final manuscript received October 30, 2017; published online December 21, 2017. Assoc. Editor: Guillaume Fromentin.

1 Introduction

Titanium alloys, such as Ti–6Al–4V (Grade 5), are extensively used in various advanced applications including medical implants and other prosthetic devices due to their excellent mechanical and physical properties [1]. Due to the addition of alloying elements, such as aluminum and vanadium, however, there are concerns about their possible alloying element diffusion–induced biotoxicity [2]. This is of particular importance for dental and medical implants, which have direct contact with bone, tissue, or bodily fluids [2]. Recently, commercially pure, coarse-grained titanium (CG Ti) is being increasingly considered as a viable alternative to titanium alloys due to the absence of biotoxic alloying elements [3]. However, CG Ti does not have enough mechanical strength as titanium alloys for many medical applications, and if CG Ti is to be used as a viable biomaterial to substitute for titanium alloys, its mechanical performance must be improved.

Fortunately, severe plastic deformation (SPD) processing, which imposes large strains on various engineering metals, enables CG Ti to have comparable mechanical strength to that of commonly used titanium alloys. The two most popular SPD processes are equal channel angular pressing ([4])/equal channel angular extrusion (ECAE [5]) and high-pressure torsion [6]. SPD processing results in an ultrafine grained (UFG) material consisting of a refined microstructure having submicron grain sizes. SPD processing improves the mechanical strength while retaining the attractive biocompatible nature of CG Ti. Generally, the drastic grain refinement results in changes in the mechanical properties such as the yield strength, ductility, and fatigue life and physical properties such as the corrosion and wear resistance, as well as thermal conductivity. Since SPD processing usually produces billets or disks, secondary machining/forming operations are usually required to further make them into final commercial or consumer products. Due to the promising application of SPD-processed UFG materials into the medical industry and the need for further post-SPD machining, it is of importance to understand the chip morphology and corresponding chip formation mechanism during UFG material machining.

The objectives of this study are to investigate the differences in chip morphology when machining ECAE-processed UFG and CG Ti and further elucidate its associated chip formation mechanism. The chip morphology is characterized according to its cross-sectional geometry using cutting speeds from 0.1 to 10 m/s. The chip formation mechanism is investigated using in situ high-speed imaging for cutting speeds of 0.1 and 0.5 m/s. Metallographic analysis of the machining chips' free surfaces, nano-indentation across the primary shear zone (PSZ), and digital image correlation (DIC) are implemented to further investigate the chip formation mechanism. Each chip formation mechanism can be correlated with its corresponding chip morphology. Since both the chip morphology and chip formation progression are dependent on the dynamic material response within the primary and secondary shear zones, the resulting understanding can be used as a starting point for developing improved high strain rate relevant constitutive models that are relevant under machining conditions. Moreover, this knowledge can be utilized to help efficiently machine Ti and its alloys, and the methodology can be easily applied to develop models for other engineering materials.

2 Background

Ultrafine grained materials are formed using a thermomechanical processing method such as inert gas condensation [7] or high-energy ball milling [8]. However, these methods are unattractive for producing large, fully dense samples due to porosity or impurities introduced during processing. In addition, the processing parameters for these methods are alloy specific and are only capable of producing grain structures in the 1–10 μm range [9]. These limitations have led to the development of SPD-processing methods, which can refine the microstructure to the submicron level by imposing large strain deformations to bulk metals. SPD-processing methods induce large plastic strains within the bulk microstructure, which subdivides large grains via dislocation pile up or a recrystallization mechanism. Although it is not applicable to process bulk metals, it should be noted that UFG materials can be produced using large strain deformation machining (this is not applicable to process bulk metals) in addition to the aforementioned equal channel angular pressing [4]/ECAE [5,10] and high-pressure torsion [6]. The processed material has enhanced mechanical and physical properties compared to unstrained material. The substantial change in the bulk microstructure of SPD-processed materials is expected to alter the deformation characteristics, especially at high strain rates. As a result, the chip formation mechanism and resulting chip morphology are expected to be different compared with a CG counterpart. Since secondary machining is usually indispensable for SPD-processed UFG materials, it is of importance to understand their machining performance in terms of the chip morphology and chip formation mechanism, in particular.

Several studies have been devoted to the machining of SPD-processed UFG materials and compared the machining performance of UFG materials with those of CG materials. Morehead et al. [11] compared the machinability of SPD-processed and CG Ti under a wide range of cutting conditions: the radial component of cutting force was found to be approximately 25% higher when cutting the SPD-processed Ti while there were no pronounced differences in tool wear and chip morphology. Morehead et al. [12] further studied the machinability of ECAE-processed UFG copper and reported a reduction in both tool wear and surface roughness. Antonialli et al. [13] measured the cutting forces, tool wear, and surface roughness to evaluate the difficulty in machining ECAE-processed Ti. The main cutting and feed forces were found to be the largest for the ECAE-processed Ti, which were nearly double that of bulk CG material and even slightly higher than the Ti–6Al–4V alloy. Similarly, both the tool wear and surface roughness increased as a result of SPD processing, indicating a reduction in the overall machinability of the ECAE-processed Ti. These results contradict what was found previously by Morehead et al. [11] and may be due to differences in the routes adopted during SPD-processing and/or the cutting tool used. Lapovok et al. [14] studied the thermal properties of ECAE-processed Ti and found a reduction in the thermal conductivity of SPD-processed materials. It was found that the change in thermal properties resulted in a serrated chip morphology at the free surface and the serration spacing of the SPD-processed Ti was smaller when compared with that of CG Ti. Davis et al. [15] studied the chip morphology during machining ECAE-processed grade 4 Ti at some selected cutting speeds and found the chip morphology to transition from saw-tooth to continuous as cutting speed increased. Despite these previous efforts to appreciate the machining performance of SPD-processed UFG materials, the underlying chip formation mechanism during machining, in particular, has been largely ignored and not investigated.

Generally, the chip formation mechanism is classified due to adiabatic shear localization [16,17] or crack initiation and propagation [18]. Adiabatic shear localization occurs when the rate of thermal softening exceeds the rate of work hardening and manifests inside a thin region known as a shear band. Crack initiation occurs when the shear stress at the free surface is a maximum prior to propagation along the primary shear plane. Accordingly, each chip formation mechanism manifests itself in different chip morphologies. Previously, the majority of research efforts on chip formation mechanisms have adopted a quick-stop approach, which abruptly removes the cutting tool from the cutting edge, leaving only a partially formed chip [19]. The arrested chips are then analyzed using postmachining metallographic analysis. However, the use of quick-stop devices and postmachining metallurgical analysis present several challenges for the understanding of chip formation process. First, quick-stop devices abruptly remove the cutting tool from the cutting edge by mechanical or explosive retraction. The abrupt removal may induce unwanted disturbances, which can initiate cracking or other undesirable perturbations.

Second, metallurgical analysis, while necessary, may produce erroneous results by removing important features of the chip morphology during sample preparation. Thus, in order to gain further insight into the chip formation process, in situ inspection of the chip formation progression together with postmachining metallographic analysis is needed, which helps identify the underlying chip formation mechanism when machining SPD-processed UFG Ti.

In order to study the chip formation process in situ, high-speed imaging has been adopted as an enabling tool [20–23] because it is advantageous over quick-stop devices by providing instantaneous snapshots of the chip formation progression without the undesirable effects of abrupt cutting tool retraction. However, the vast majority of prior work utilizing high-speed imaging-based systems use plane strain sliding experimental setups where the workpiece moves relative to a fixed cutting tool (similar to planing) to mimic the machining process. As such, the cutting process is actually interrupted with each machining stroke such that cutting may not be under steady-state conditions. It is unclear if the resulting chip formation mechanism studied during plane strain sliding remains the same as during conventional metal cutting. Ideally, such high-speed imaging evaluations should be conducted using an actual machining setup.

3 Materials and Methods

3.1 Materials. In this study, CP CG grade 4 Ti (CG 4, Service Steel Aerospace Corp., Seattle, WA) was selected for SPD (ECAE) processing using the method outlined in Ref. [10], and the resulting ECAE-processed Ti bars were further used to investigate the chip formation mechanism and chip morphology during machining. In particular, the ECAE Ti bars, denoted ECAE 1 and ECAE 2, were processed using route $4B_c$ (90 deg rotation about the long axis for four passes) at 320 °C on $25 \times 25 \times 150$ mm bars. Extrusion speeds of 0.05 m/s and 0.01 m/s were used for all extrusion passes for ECAE 1 and ECAE 2, respectively. The thickness of ECAE 1 was reduced by approximately 6% by rolling between extrusion passes, while no additional rolling was used for ECAE 2. The ECAE processing conditions for each specimen are also summarized in Table 1.

Under these conditions, the ECAE processing led to a substantial reduction in grain size (approximately 200 nm of the ECAE Ti bars compared with 10–20 μm of the CG Ti bars [2,14]). Both the ECAE and CG Ti bars, originally square, were machined down to 25 mm in diameter and further used in orthogonal machining experiments, which were designed to elucidate possible differences in the chip morphology and chip formation mechanism.

3.2 Machining Setup. The machining experiments were conducted with two different machine tools under an orthogonal dry cutting configuration using an uncoated tungsten carbide grooving tool (NG3125R K313, Kennametal, Latrobe, PA). A manual Whacheon HL 435 lathe (Whacheon, Huntington Beach, CA) was used to elucidate the chip formation mechanisms during low-speed machining (0.1–0.5 m/s) whose open space enabled the high-speed imaging of the chip formation process. This cutting speed range was chosen to facilitate high-speed imaging studies by avoiding damaging imaging lens at a short focal length (approximately 50 mm herein) due to high cutting temperatures and providing quality images for DIC analysis. In addition, a computer numeric control Mikron UCP 600 Vario machining center (Georg Fischer AG, Schaffhausen, Switzerland) was used to evaluate the chip morphologies during high-speed machining (up to 10.0 m/s). It should be noted that differences in machine tool rigidity may result in variations in machining dynamics. As such, the chip morphology from both machine tools, produced at the same cutting speed, was compared, and the difference was found insignificant. The feed rate and depth of cut were held constant at 0.1 mm/rev and 2.0 mm, respectively, while the cutting speed varied from 0.1 to 10.0 m/s. The cutting conditions used in the present study are chosen to evaluate the effect of a wide range of cutting speeds even that some cutting speeds within this range may be beyond those suggested by the tool manufacturer and those used in industry. The effective tool rake angle was held at 0 deg, and a new cutting tool was used for each cutting speed.

Table 1 Processing parameters for ECAE processing (processing temperature at 320 °C and rotation angle of +90 deg)

	Extrusion speed (m/s)				
Materials	N1	N2	N3	N4	Comments
ECAE 1	0.05	0.05	0.05	0.05	Rolled 6% between extrusions
ECAE 2	0.01	0.01	0.01	0.01	Not rolled between extrusions

For the Whacheon manual lathe-based chip formation study, the Ti workpiece was in the form of a disk produced from the 25 mm square cross section bars. Each disk was prepared by machining a grove 2.0 mm from an end of the disk sample as shown in Fig. 1(*a*). During machining, the tool fed radially toward the axis of rotation, simulating an orthogonal cutting configuration. A high-speed camera system (Photron SA-5, San Diego, CA), aligned along the axial direction and focused on the PSZ, was used to capture the chip formation process. The camera system was mounted directly to an adjustable *XY* fixture attached to the linear slide, which guaranteed the camera motion synchronized with that of the cutting tool during machining. The Photron camera system has a 12-bit ADC CMOS censor with a 1024×1024 pixel resolution. During the machining test, frame rates up to 50,000 fps were used to image the deformation of the PSZ. For better imaging results, a Navitar zoom lens system (Navitar, Rochester, NY) was used with the high-speed camera system by adding a 1× lens attachment and a 2× lens extender, resulting a final magnification, spatial resolution, and field of view of approximately 15×, 3 μm, 0.5×0.5 mm^2, respectively. The focal length of the lens was approximately 50 mm. Fine focus was achieved by manual adjustment on the lens. In addition, two SugarCUBE LED-based light sources (Nathaniel Electronics, Vergennes, VT) were used to illuminate the cutting area of interest: one SugarCUBE was coupled with the Navitar lens system using coaxial illumination and the other was used as an external light source. The experimental setup is shown in Fig. 1(*b*).

3.3 Postprocessing of Machining Chips. After machining, the chips were collected and cast in a low-viscosity epoxy (Pace Technologies, Tucson, AZ) to characterize chip morphology. First, the cast chip samples were mechanically ground using SiC sandpaper with grits from 600, 800, 1000, and 1200 successively for approximately 5 min each. Following mechanical grinding, the samples were polished using a 1 μm polycrystalline diamond solution for 20 min. The final polishing step utilized a 0.05 μm alumina solution until a mirror finish was achieved. The time for the final polishing step was typically 20 min. The chip samples were then etched using Kroll's reagent (92 mL DI-H_2O, 6 mL HNO_3, 2 mL HF) (Sigma-Aldrich, St. Louis, MO) for approximately 20 s to reveal fine features in the microstructure to aid in classifying different chip morphologies. Finally, scanning electron microscopy (SEM) (Phenom ProX, NanoScience Instruments, Alexandria, VA) was used to image the chip morphology. The shear band spacing and shear angle [24] were measured directly from the SEM images. The average shear band spacing was determined by taking five successive shear band spacing measurements from five different chips at each cutting speed.

In addition, the hardness of the Ti machining chips was measured by mounting in epoxy and characterized with a Hysitron™ TI Premier indenter (Hysitron, Minneapolis, MN) equipped with a Berkovich tip (Hysitron, Minneapolis, MN). After quasi-static nano-indentation, the loading-unloading curves were analyzed

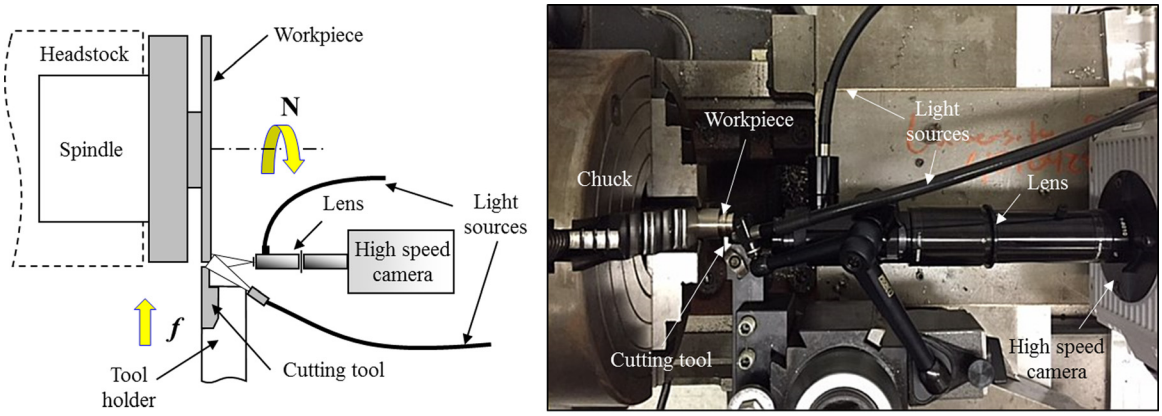

Fig. 1 (*a*) Schematic representation of the experimental setup and (*b*) high-speed camera system implemented on the Whacheon lathe

using the method proposed by Oliver and Pharr [25]. Three-row indentation arrays were carried out perpendicular to the shear bands on the chips with each indent spaced 5 μm apart. A peak load of 4000 μN and a 5 s peak load holding time were used during the analysis. Each indent was separated by more than ten times their depth, which ensured they would be unaffected by neighboring indents. Using the three-row arrays, averages and standard deviations were calculated for each column corresponding to a discrete distance from the shear band. In some cases, unloading curves exhibited behavior characteristic of false engagement on the sample surface. In these cases, the clearly erroneous curves were eliminated from statistics calculations. The resulting data were used to describe the hardness as a function of distance from the shear band in the machined chips.

4 Results and General Discussion

4.1 Chip Morphology. The chip morphologies of both ECAE 1 and ECAE 2 machined in the cutting speed range of 0.1–10.0 m/s are shown in Fig. 2 (cross-sectional view) and Fig. 3 (free surface view). In general, the machining chips can be classified into three chip morphologies: aperiodic saw-tooth chips, continuous chips, and periodic saw-tooth chips. As suggested by Barry and Bryne [26], aperiodic and periodic saw-tooth chips are differentiated using the surface topography of the saw-tooth segments. Herein, if the saw-tooth segments extend continuously through the chip width, the saw-tooth chip morphology is considered periodic, whereas if the saw-tooth segments are interrupted through the chip width, the saw-tooth chip morphology is considered aperiodic. Representative chip surface topographies of machining chips at different cutting speeds are shown in Fig. 3.

As shown in Fig. 2, the chip morphology of both ECAE-processed Ti workpieces is aperiodic saw-tooth at a cutting speed of 0.1 m/s while the chip free surface looks like folds. This chip morphology has been frequently reported during machining of Ti [27,28] and its alloys [26,29]. As the cutting speed is increased to 0.5–1.0 m/s, a continuous chip morphology is apparent. The continuous chip morphology is common during machining of ductile metals for cutting speeds less than 2 m/s [30]. This transition from aperiodic to continuous chips indicates that a different chip formation mechanism is operative as the cutting speed increases. Further increase of the cutting speed to 2.5 m/s results in the formation of periodic saw-tooth chips, which indicates that a second transition in the chip formation mechanism occurs. Periodic saw-tooth chips remain the primary chip morphology up to 10.0 m/s. It is worth mentioning that discontinuous chips are commonly formed if sufficiently large cutting speeds are used [30]. From Fig. 2, little difference between the chip morphologies for ECAE 1 and ECAE 2 is observed, illustrating the 6% rolling condition may not result in a pronounced effect in the chip morphology.

For comparison, the chip morphology of the CG grade 4 Ti is also shown in Fig. 2. Similar to the ECAE-processed Ti, the chip morphology at the cutting speed of 0.1 m/s is aperiodic saw-tooth. In contrast, as the cutting speed increases to 0.5–1.0 m/s, the aperiodic saw-tooth chip morphology remains, which indicates that the chip formation mechanism differs from that during ECAE-processed Ti machining. When the cutting speed increases to 2.5–10.0 m/s, the periodic saw-tooth chip formation dominates. The primary difference in the chip morphologies between the ECAE-processed Ti and CG Ti occurs within the cutting speed range from 0.5–1.0 m/s. Within this range, the chip morphology of the ECAE-processed Ti is continuous, while the aperiodic saw-tooth chip morphology is observed for the CG Ti. Thus, ECAE-processing alters the dynamic deformation response of the Ti, which is indicated by the transition in the chip morphology from aperiodic saw-tooth to continuous as the cutting speed increases during the cutting speed range of 0.5–1.0 m/s.

4.1.1 Shear Band Spacing. For each chip morphology shown in Fig. 2, the shear band spacing at each cutting speed was measured experimentally from postmachining metallographs. Since no pronounced shear bands are observed in the ECAE-processed Ti when machining at 0.1 m/s, the saw-tooth segment spacing is used for comparison purposes. In addition, the shear band spacing for the continuous chip morphology is assumed to be infinitesimally small and is reported to be zero. Figure 4 shows the measured shear band spacing of both the ECAE-processed Ti and CG Ti chips. In general, the shear band spacing increases with the cutting speed for both ECAE-processed Ti and CG Ti chips, which agrees well with previous reports during machining of CG materials [24,31]. Compared with the CG Ti chips, the shear band spacing is always smaller for the ECAE-processed Ti chips, owing to the reduction in grain size and difference in material response at higher strain rates. This observation agrees well with the results reported during machining of SPD-processed Grade 2 Ti [14]. Comparing the two ECAE-processed Ti chips, the shear band spacing increases at the same rate; however, the shear band spacing of the ECAE 1 chips is slightly higher than that of the ECAE 2 chips. This result may be due to the differences in the ECAE-processing conditions; however, the measurements are within the one-sigma standard deviation and the difference is considered negligible.

Molinari et al. [31] considered the shear band spacing as a function of cutting speed and thermal properties, in particular, the thermal softening coefficient and thermal conductivity. Lapovok et al. [14] investigated the thermal properties of ECAE-processed Ti

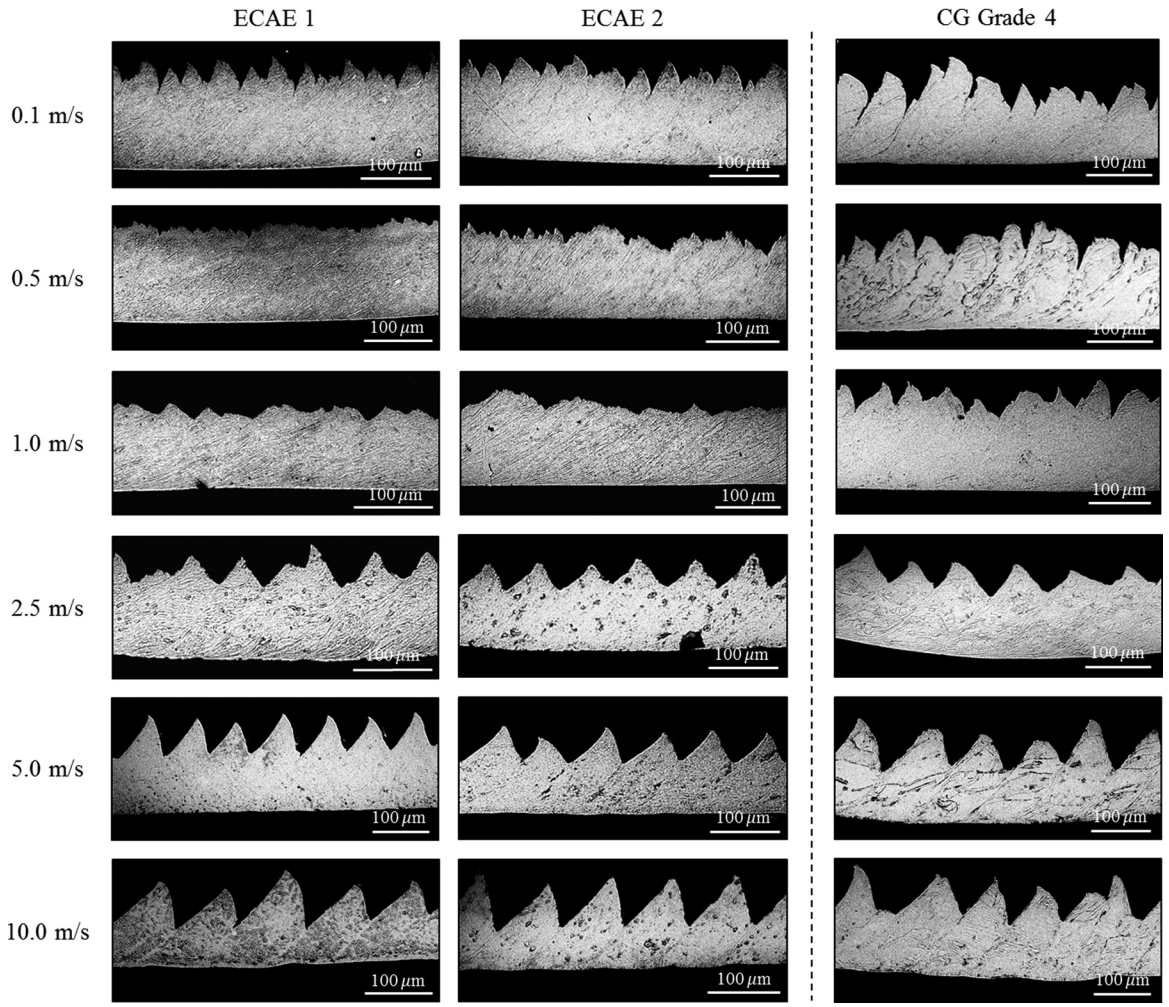

Fig. 2 Representative chip morphology variations of ECAE 1, ECAE 2, and CG grade 4 Ti chips as a function of cutting speed

and found a reduction in thermal conductivity. The thermal softening effect intensifies due to the increased thermal generation at high cutting speeds during ECAE Ti machining. During machining, shear band formation occurs when the rate of thermal softening exceeds the rate of work hardening [17]. As such, ECAE-processed materials should be more susceptible to shear band formation, resulting in a smaller shear band spacing. Because the microstructure of ECAE-processed materials is already refined, machining, as an SPD process, may not be able to further refine their microstructure. Under certain cutting conditions such as the cutting speed of 0.5–1.0 m/s, ECAE-processed Ti accommodates excess deformation and reduces the tendency for shear band formation, resulting in the continuous chips, and it calls for further metallurgical examination of this phenomenon.

4.1.2 Degree of Segmentation. The degree of segmentation (G), which is a ratio of the maximum and minimum thickness (peak-to-valley thickness) of the chip cross section, can be measured using the procedure described elsewhere [32,33] as follows:

$$G = \frac{h_1 - h_2}{h_1} \tag{1}$$

where h_1 is the peak chip height and h_2 is the chip valley height between two adjacent segments. When the degree of segmentation is 0, this indicates continuous chip formation, whereas as G approaches 1 the chips turn to be discrete, discontinuous segments. As shown in Fig. 5, when the cutting speed increases, the degree of segmentation increases for both the aperiodic and periodic saw-tooth chips.

At low cutting speeds when the aperiodic saw-tooth chip morphology is observed, CG Ti has the largest degree of segmentation. This observation is possibly due to the high ductility of the CG Ti at low cutting speeds, which facilitates segment sliding during the saw-tooth chip formation process. Since the reduction in thermal conductivity may result in increased ductility at higher cutting speeds due to thermal softening, longer sliding distances may occur during saw-tooth chip formation. As the cutting speed increases, periodic saw-tooth chips are observed for the ECAE-processed Ti, which has the largest degree of segmentation. As with the shear band spacing, the degree of segmentation for ECAE 1 is slightly higher than that of ECAE 2.

4.2 Chip Formation Progression. As shown in Fig. 2, a distinct transformation in chip morphology occurs for the ECAE-processed Ti when increasing the cutting speed from 0.1 m/s to 0.5 m/s and again from 1.0 to 2.5 m/s. This indicates that the dynamic material response, in terms of the chip formation mechanism, changes with cutting speed. Each chip morphology is a direct result of a specific chip formation mechanism such as uniform (homogeneous) shear deformation [19,30], adiabatic shear localization [17,34], and crack initiation and propagation [18,27]. Moreover, the second chip morphology transition of ECAE Ti occurs at a cutting speed of 2.5 m/s, which is very difficult to image with high spatial resolution. Therefore, the in situ investigation of chip formation progression using high-speed imaging is

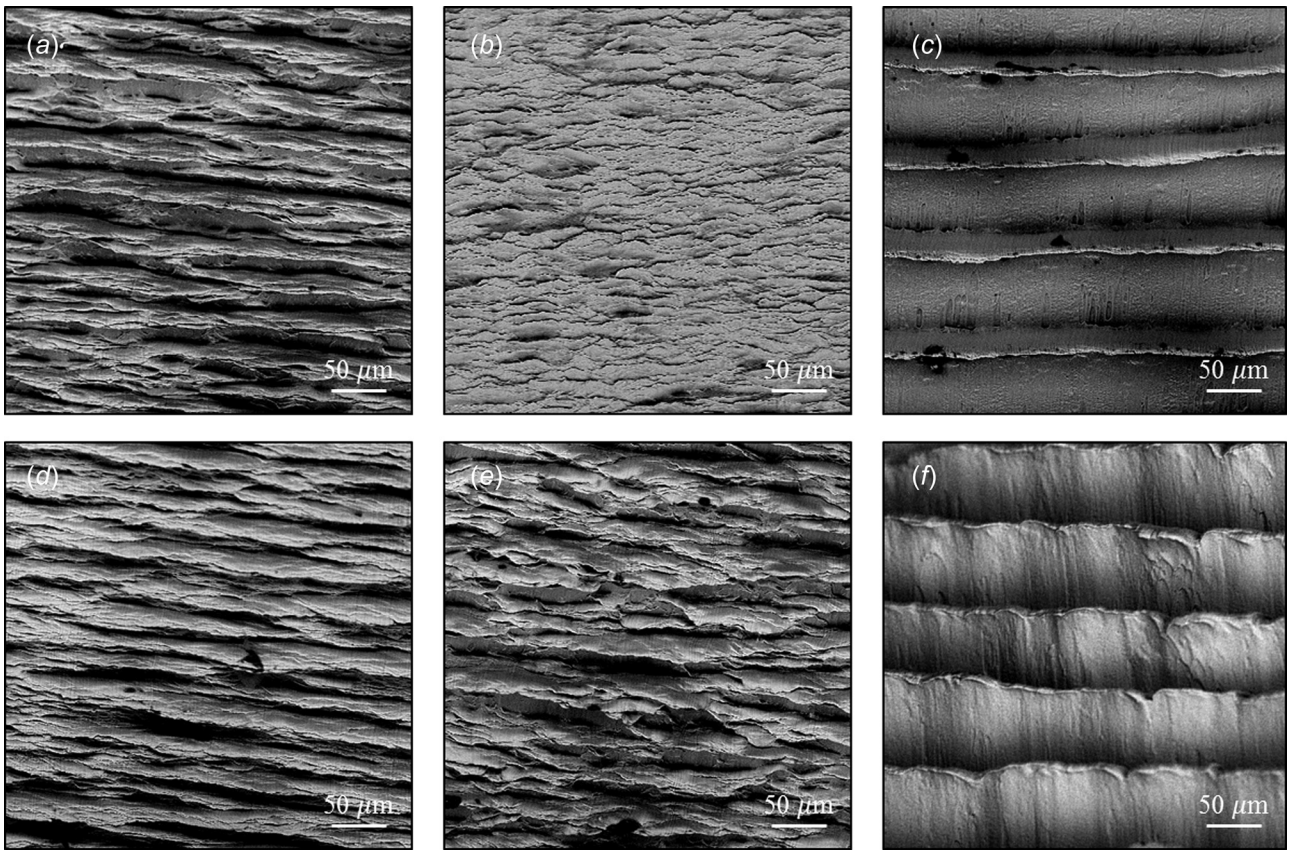

Fig. 3 Surface topographies of ECAE-processed Ti chips (perpendicular to the chip surface): (*a*) aperiodic saw-tooth chip formation (0.1 m/s), (*b*) continuous chip formation (0.5 m/s), and (*c*) periodic saw-tooth chip formation (10 m/s). For comparison, the corresponding surface topographies of CG Ti chips are also shown in (*d*)–(*f*).

only carried out in the range $0.1 \leq V_c \leq 0.5$ m/s, even though these cutting speeds may not be high for Ti and its alloys.

4.2.1 Saw-Tooth Chip Formation (V = 0.1 m/s). Figure 6 shows a representative image sequence of the chip formation progression of a single saw-tooth segment during machining of ECAE-processed Ti using a cutting speed of 0.1 m/s. In general, four stages of deformation can be identified: (1) wedge-shaped compression, (2) free surface upsetting, (3) instability, and (4) segment sliding. Stage 1 is depicted in Fig. 6(*a*) where a wedge-shaped volume of material ahead of the cutting tool, delineated by Line OA, enters the PSZ and is compressed against the tool rake face. During this stage, the frictional force in the secondary shear zone and the affinity between the cutting tool and workpiece material increases the tendency for sticking at the tool tip, which results in the formation of a cyclic built up edge (BUE). The formation of a cyclic BUE at the tool tip increases the local shear strain and forces the material at the free surface to rise above the horizontal plane (along Line AB) as shown in Fig. 6(*b*). A closer examination of Fig. 6(*b*) reveals what likes look a notch already formed at the free surface during stage 2, which is actually due to the imaging quality-induced perception. Material failure is still under its development during the second stage, which distinguishes it from

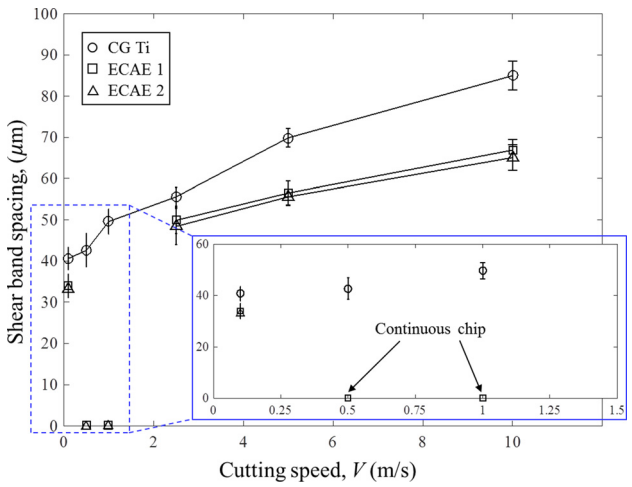

Fig. 4 Shear band spacing of ECAE-processed and CG Ti chips (± sigma error bars)

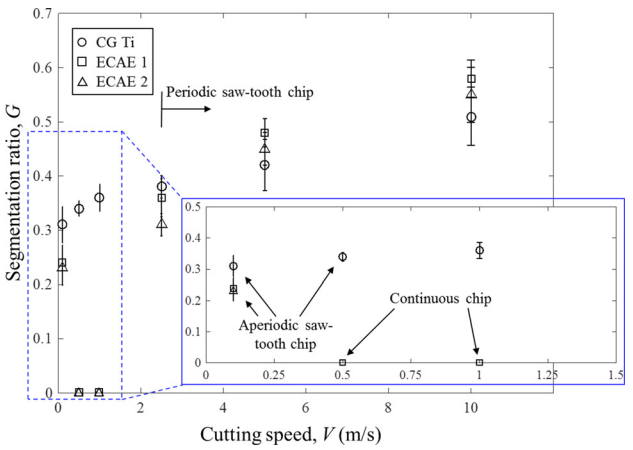

Fig. 5 Segmentation ratio of ECAE-processed and CG Ti chips (± sigma error bars)

stage 3. This is known as free surface upsetting and has been reported to be a precursor to instability during saw-tooth chip formation [35]. Free surface upsetting concludes with the initiation of instability in the form of shear localization within the PSZ as shown in Fig. 6(*c*). As with many other studies, the instability is assumed to initiate at the tool tip (point O) and propagate toward the free surface to Point A' [17,26,30,34]. Instability occurs due to the reduction in flow stress within a localized region. Consequently, this region is weakened and is the preferred sliding direction during segment sliding along the adjacent workpiece as shown in Fig. 6(*d*). As observed, the relative sliding between adjacent segments is the main contributor to the overall shear strain within the shear localized region. Generally, the relative sliding is modeled as two linear sliders moving relative to each other, acting as an additional thermal source. If their temperature is sufficiently high, dynamic recrystallization ensues, and pronounced shear bands are clearly visible in the chip microstructure. Thus, the lack of such metallographic features indicates that shear localization does not lead to the formation of well-defined shear bands herein. Moreover, while there are no observable shear bands in the microstructure, the absence of observable cracks in the high-speed image sequences or in the chip metallographs indicates that cyclic (inhomogeneous) shear localization is the primary chip formation mechanism rather than crack initiation and propagation as typically reported during machining of CG Ti [27]. It should be pointed out that the chip formation phenomenon can also be simplified as a three stages progression: compression, shear instability, and sliding.

4.2.2 Continuous Chip Formation ($V = 0.5$ m/s). Figure 7 shows a representative image sequence of the chip formation progression of the continuous chip morphology during machining of ECAE-processed Ti at a cutting speed of 0.5 m/s. In general, the most significant difference between the continuous and saw-tooth chip formation is that no segmentation occurs (i.e., no instability or segment sliding) during continuous chip formation. Figure 7(*a*) shows that a parallelogram-shaped volume of material, delineated by OABC, flows from the workpiece and into the PSZ where it is compressed against the tool rake face. This is similar to stage 1 of deformation during saw-tooth chip formation. However, the primary difference is that the increase in both strain rate and temperature suppresses the formation of a cyclic BUE as shown in Fig. 7(*b*). As such, material upsetting does not occur, and the local cutting temperature increase improves the ductility, which hinders segmentation. As chip formation process continues, all the incoming workpiece material is elongated uniformly along the shear direction. Figure 7(*c*) shows an undeformed element and the corresponding deformed element once the material passes through the PSZ. During machining of CG materials, increases in the cutting temperature and strain rate facilitate shear localization due to thermal softening within the PSZ [30]. However, for ECAE-processed Ti, excess deformation is accommodated under high strain rate and temperature conditions; the material is uniformly deformed as it travels through the PSZ, and segmentation is suppressed. Grain elongation can also be observed microscopically in the chip metallographs shown in Fig. 2. Therefore, it is concluded that the chip formation mechanism for ECAE-processed Ti at 0.5 m/s is due to uniform shear localization. The differences between this mechanism and cyclic shear localization, which is the primary chip formation mechanism during saw-tooth chip formation, will be discussed further in Sec. 5.

Generally, differences in the material response within the PSZ result in different chip formation mechanisms and chip morphologies. As observed, the ECAE-processed Ti forms a saw-tooth chip by cyclic shear localization at a cutting speed of 0.1 m/s. Increasing the cutting speed to 0.5 m/s produces a transition in chip formation mechanism to uniform shear localization. Comparing with the chip formation progression for CG Ti, the chip formation mechanism within this cutting speed range ($0.1 \leq V_c \leq 0.5$ m/s) is due to cyclic shear localization, and no transition of chip morphology is observed. While notable changes in the chip formation mechanism are discussed from a macroscopic perspective based on the high-speed images, microstructural phenomena responsible for differences in the chip formation mechanism during ECAE Ti machining are further investigated in Sec. 5.

5 Discussion on Chip Morphology and Chip Formation Mechanism

In general, ECAE processing leads to a substantial reduction in grain size, with commensurate increases in yield strength and hardness and a decrease in ductility at room temperature. The microstructure of such SPD-processed materials contains significant lattice distortions associated with high internal stresses, poorly defined grain boundaries, and a high dislocation density [36]. Moreover, deformation twins in high densities have been reported in ECAE-processed Ti [37]. These microstructural factors suggest that the deformation mechanisms of ECAE-processed Ti may differ from those governing CG Ti. In addition to the aforementioned chip formation differences between the ECAE-processed and CG Ti based on the chip morphologies and high-speed image sequences, such differences are further examined using the chip free surface, DIC [38–40], and nano-indentation.

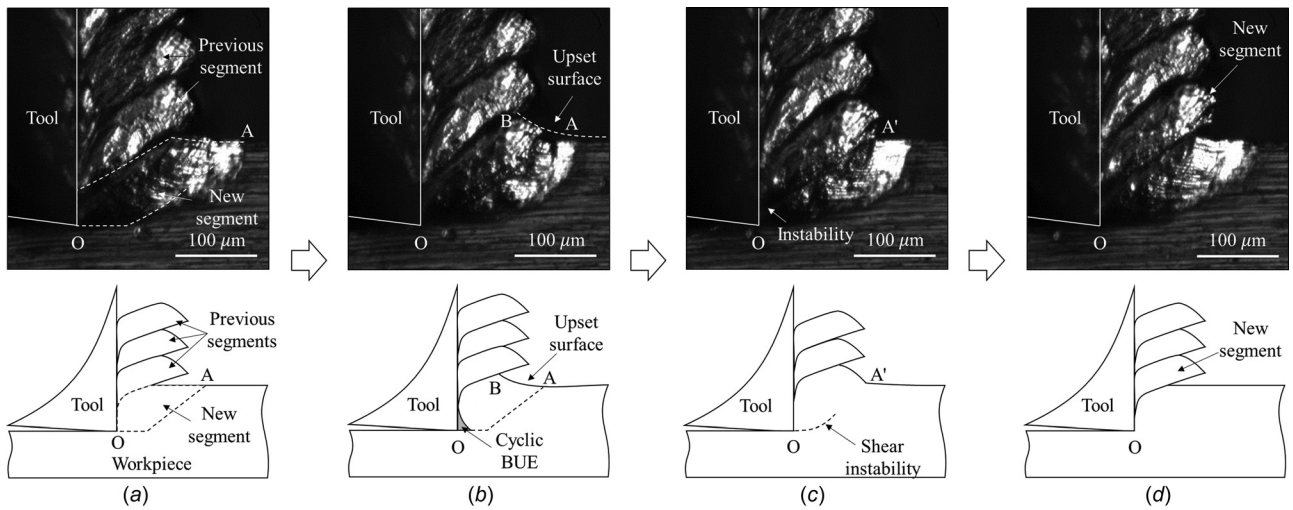

Fig. 6 Progression of a single saw-tooth segment of ECAE-processed Ti machined at a cutting speed of 0.1 m/s. The schematics illustrate the four deformation stages: (*a*) stage 1, (*b*) stage 2, (*c*) stage 3, and (*d*) stage 4.

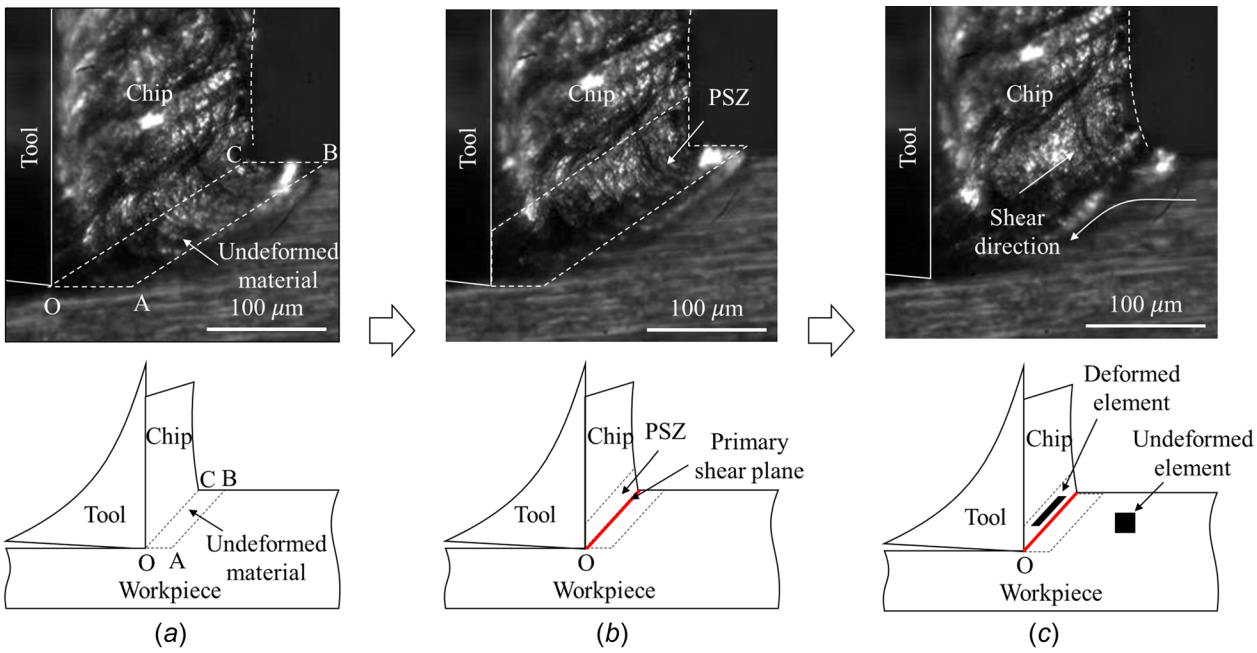

Fig. 7 Progression of continuous chip formation of ECAE-processed Ti machined at a cutting speed of 0.5 m/s

5.1 Chip Morphology

5.1.1 Topographical Free Surface. In addition to instantaneously imaging the chip formation progression at incremental time steps, the free surfaces were examined to provide insight into the microstructural mechanisms responsible for the formation of different chip morphologies. In this study, the microstructural features on the chip free surfaces obtained at the cutting speeds of 0.1, 0.5, and 10.0 m/s are inspected using SEM where the viewing direction is perpendicular to the free surface as shown in Fig. 8(*a*). These cutting speeds were selected to show the differences in the free surfaces due to the change in the chip formation mechanism as the cutting speed increases.

Figure 8 shows the free surfaces of both ECAE 1 and CG Ti at the aforementioned cutting speeds. Since little difference in the chip morphology is observed for ECAE 1 and ECAE 2, the chip formation mechanism is assumed to be the same, and only the free surfaces for ECAE 1 are presented. In general, the free surfaces show several distinct textures such as rippled texture, smooth surface, and elongated dimples. Figures 8(*b*), 8(*e*), and 8(*f*) shows the free surface of the aperiodic saw-tooth chip morphology formed by cyclic localized shearing for ECAE-processed Ti and CG Ti, respectively. These free surfaces are very similar in texture, and the chip formation mechanism is assumed to be the same. The rippled texture arises due to ductile shear and is elongated along the chip flow direction, which is due to the relative sliding between a segment and its adjacent workpiece. Figure 8(*c*) shows the free surface of the continuous chip morphology formed by uniform shear localization. As shown, the free surface with fine lamellae differs from that of the aperiodic saw-tooth chip. These fine lamellae are assumed to be due to the moving shear front as the microstructure is deformed uniformly [26,41]. Figures 8(*d*) and 8(*g*)

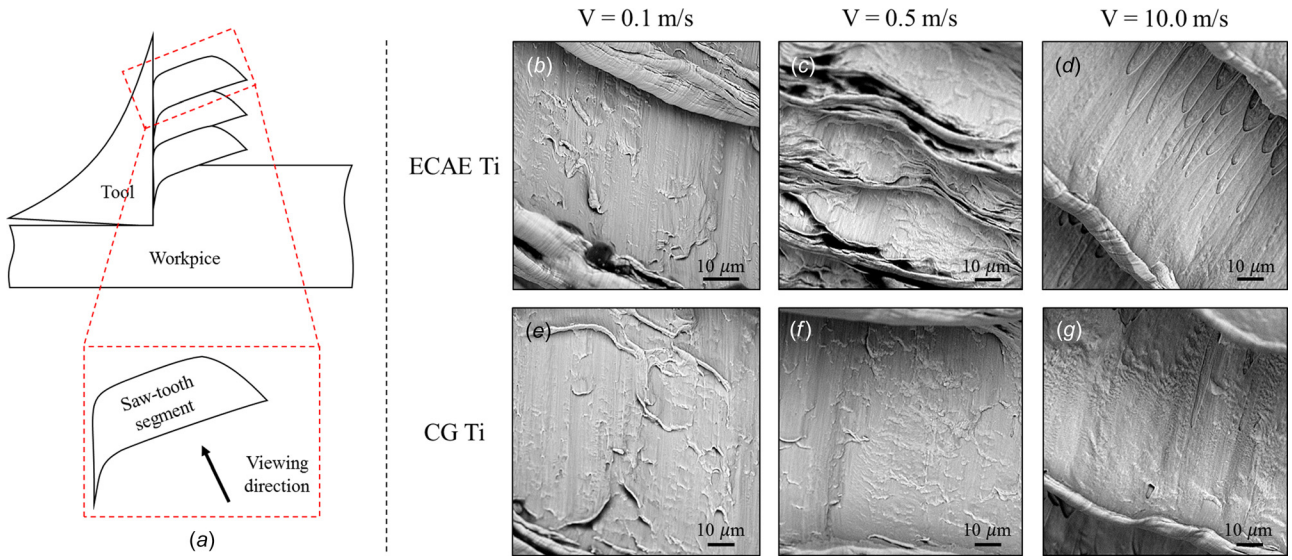

Fig. 8 Free surfaces of ECAE-processed Ti chips: (*a*) schematic of a saw-tooth segment showing the viewing direction, (*b*) rippled texture at 0.1 m/s, (*c*) fine lamellae at 0.5 m/s, and (*d*) smooth surface/elongated dimples at 10.0 m/s. For comparison, the corresponding free surfaces of the CG Ti chips are also shown in (*e*)–(*g*).

shows the free surface of the periodic saw-tooth chip morphology machined at the cutting speed of 10.0 m/s. Two distinct textures are readily observed: a smooth surface in the upper region of the PSZ, and elongated dimples in the lower region. Generally, a smooth free surface is indicative of a brittle deformation mechanism resulting from crack initiation and propagation. Gu et al. [42] suggested that this smooth texture occurs due to a rapidly moving sharp-tip crack within a transformed shear band. It is possible that the intense thermal generation due to the high cutting speed is sufficient to result in thermal softening and even a phase transformation within the shear band. The phase transformation would result in a loss in ductility, which facilitates crack propagation [35]. The texture on the free surface within the lower region of the PSZ consists of large elongated dimples, which occur due to ductile fracture. The elongation occurs due to the intense thermal generation at the tool tip and the relative sliding between a segment and its adjacent workpiece. Such elongated dimples have been reported elsewhere during machining of Ti–6Al–4V Ti alloy [26] and AISI 1045 hardened steel [43].

5.1.2 ECAE-Processed Ti Chip Microstructure. It has been recognized that saw-tooth chip formation occurs primarily by adiabatic shear localization and manifests in localized bands known as shear bands [35]. In other works, the appearance of shear bands has been used as an indicator to suggest that adiabatic shear localization is the operative chip formation mechanism [34]. Usually, the microstructure inside a shear band consists of a highly refined grain structure, which may be attributed to the recovery/recrystallization mechanism. Thus, the formation of such microstructural features requires specific levels of strain, strain rate, and temperature. While no pronounced shear bands are observed in the ECAE Ti chip metallographs at the cutting speed of 0.1 m/s as shown in Fig. 2, this does not discount the adiabatic shear localization mechanism; rather, it indicates that other microstructural factors contribute to the chip formation process. The substantial grain size reduction resulting from ECAE-processing produces a nonequilibrium grain structure, which gives rise to possible grain boundary sliding, dislocation motion, and/or superplasticity at high strain rates and relatively low temperatures to accommodate excess deformation [44] and might be related to the suppression of shear bands within the PSZ. As such, adiabatic shear localization may still be the chip formation mechanism while there are no pronounced shear bands seen in the chips of during ECAE-processed Ti.

Increasing the cutting speed to 0.5 m/s results in a change in the chip morphology of the ECAE Ti, indicating a change in chip formation mechanism. Generally, increases in the cutting speed show an increased propensity for the formation of saw-tooth chips [30]. However, this phenomenon is not observed during machining of ECAE-processed Ti. Instead, the chip morphology changes from aperiodic saw tooth to continuous when the cutting speed increases from 0.1 to 0.5 m/s. The increase in cutting speed, which also increases the strain rate and cutting temperature, may increase the local ductility and be responsible for the suppression of the saw-tooth formation.

While superplasticity has been reported for ECAE-processed materials, many of these studies show that it occurs under high temperatures ($T > 600$ K) and low strain rates ($10^{-4} - 10^{-2}$ s^{-1}). Ko et al. [44] suggested that possible grain boundary sliding, dislocation motion, and/or superplasticity can be an operative deformation mechanism at lower temperatures and higher strain rates (10^{-2} s^{-1}) at nonequilibrium grain boundaries within the microstructure to accommodate excess deformation. However, the strain rate during machining of SPD-processed Ti at the cutting speed of 0.5 m/s is the order of 1000 and much higher than 10^{-2} s^{-1}; it calls for a future study whether the continuous chip formation and uniform shear localization are governed by possible grain boundary sliding, dislocation motion, and/or superplasticity at nonequilibrium grain boundaries.

5.2 Chip Formation Mechanism

5.2.1 Shear Strain Rate Progression Using DIC. As shown in Fig. 6, the instability (stage 3) of the ECAE-processed Ti is attributed to cyclic shear localization, which is assumed to initiate at the tool tip and propagate toward the free surface. While there is no indication of shear localization in the form of shear bands from the high-speed images or by metallographic analysis, the possible existence of shear localization with the PSZ for both aperiodic saw-tooth and continuous chips is examined using DIC. Specifically, DIC is used to make inferences about the chip formation mechanism for ECAE Ti for cutting speeds up to 0.5 m/s based on the high-speed images using DaVis StrainMaster, a specialized DIC software package (LaVision Inc., Goettingen, Germany) using a procedure outlined elsewhere [45]. The chip formation mechanism can be analyzed using the time-dependent, incremental shear strain rate distribution.

Figure 9 shows the shear strain rate progression of chip formation during a single cycle for ECAE-processed Ti. It is noted that due to the similarities in chip morphology and free surfaces between the ECAE-processed Ti and CG Ti at the cutting speed of 0.1 m/s, the shear strain rate progression is assumed the same. Figure 9(*a*) shows the progression of a single saw-tooth segment machined at 0.1 m/s. It is evident that the position of the PSZ is not a constant and shifts in the chip flow direction as deformation progresses. Generally, the deformation during saw-tooth chip formation is localized within a thin region between adjacent bulk segments, which undergo little deformation. Thus, once the deformation is localized within the shear band, this region moves with the chip in the direction of chip flow. As seen from Fig. 9(*a*), the peak distribution at $t = 0$ ms shows the progression for stage 1, the peak distribution at $t = 0.10$ ms shows the progression for stage 2, etc., clearly illustrating the shift of the shear strain rate peak, which indicates the formation of saw-tooth segments. As observed based on those of the ECAE and CG Ti materials, the peak shift is similar through stages 1 and 2. However, once instability occurs, the peak shift is slightly larger for CG Ti, which is most likely due to the difference in the shear band spacing or segmentation ratio (Figs. 4 and 5) once the segment begins to slide along the adjacent workpiece.

Figure 9(*b*) shows the time dependent shear strain rate progression during the formation of a continuous chip over a similar period. Since continuous chips do not form with any periodicity, the time domain is chosen such that the number of frames used for Figs. 9(*a*) and 9(*b*) are the same. Due to the increase in cutting speed associated with Fig. 9(*b*), the interframe displacement is larger at the higher cutting speed; thus, the sampling period is shorter for the same number of frames studied. As hypothesized, continuous chip formation occurs by uniform shear deformation where grains are deformed along the shear direction [26,30]. This suggests that shear strain localization occurs uniformly at the same location as opposed to cyclically as during saw-tooth chip formation. Thus, criteria can be established such that for saw-tooth chip formation, the PSZ shifts in the direction of chip flow whereas for continuous chip formation, the location of the PSZ remains constant.

These observations can be further evaluated by examining the shear strain rate distributions across a larger time period. Figure 9(*c*) shows the shear strain rate distribution for the development of multiple saw-tooth segments, and Fig. 9(*d*) shows the shear strain rate development for a continuous chip using the same number of frames as with Fig. 9(*c*). As shown, even when multiple segments are produced, deformation occurs cyclically for the saw-tooth chip, indicating that the PSZ shifts in the direction of chip flow and there is a volume of relatively less deformed material (interior of segment or bulk segment) between two sequential shear bands. Additionally, the magnitude of the shear strain rate reduces as the PSZ flows away with a chip segment. On the other hand, the shear strain rate of continuous chips remains localized at a fixed position even over a longer period as shown in Fig. 9(*d*).

It should be noted that these results show the shear strain rate (and shear strain) is always localized regardless of the chip formation mechanism or chip morphology. By using DIC to analyze the shear strain rate development throughout one or several chip formation cycles, criteria to define the chip morphology and associated chip formation mechanism can be established. If the shear strain rate distribution contains a cyclic PSZ, meaning the peak in shear strain rate shifts as deformation progresses, the chip morphology is considered saw tooth. This observation agrees with previously reported work [35] and indicates the shear strain rate is localized within a thin region and its adjacent material is relatively less deformed. On the other hand, if there is relatively little peak shift in the shear strain rate distribution as shown in Figs. 9(*b*) and 9(*d*), this indicates that a continuous chip forms and while the deformation is localized, it occurs due to uniform shear or uniform shear localization and all are deformed to similar levels of strain.

5.2.2 Shear Band Hardness Evaluation Using Nano-Indentation. Adiabatic shear localization manifests itself in the form of shear bands, which are metallographic features consisting of a refined microstructure between adjacent, less refined segments. Critical cutting conditions are required for shear bands to appear in any chip. Previously, shear bands have been used as an indicator to suggest that adiabatic shear localization is the operative deformation mechanism. However, for ECAE-processed materials machined at low cutting speeds, no pronounced shear bands exist; thus, it is difficult to identify the chip formation mechanism using metallography only. In this study, microhardness measurements were conducted across the sheared region using nano-indentation. As with the free surface analysis, cutting speeds of 0.1, 0.5, and 10.0 m/s were used to investigate the microhardness associated with different chip formation mechanisms.

Figure 10 shows the variation in hardness across the shear band of both ECAE-processed and CG Ti. In general, the hardness increases across the localized shear zone, with the maximum hardness occurring inside the shear band. As shown in Fig. 10(*b*), there is a clear difference in the hardness measurements for the machining chips within the cutting speed range from 0.1 – 0.5 m/s. At the cutting speed of 0.1 m/s, two localized peaks are observed, which represent two adjacent shear bands. Thus, despite the absence of pronounced shear bands in the chip metallographs, regions of localized shear of aperiodic saw-tooth chips may still exist between adjacent segments as reflected by the hardness peaks, which are around 4.9 GPa. Increasing the cutting speed to 0.5 m/s results in a relatively constant, lower hardness (1.0 GPa), which indicates that deformation occurs uniformly through the PSZ without a less deformed bulk segment. Figure 10(*b*) also shows the hardness measurements for periodic saw-tooth chips using the cutting speed of 10 m/s. In this case, the hardness within the shear band of periodic saw-tooth chips (6.5 GPa) increases substantially compared with that of the bulk segment. Calamaz

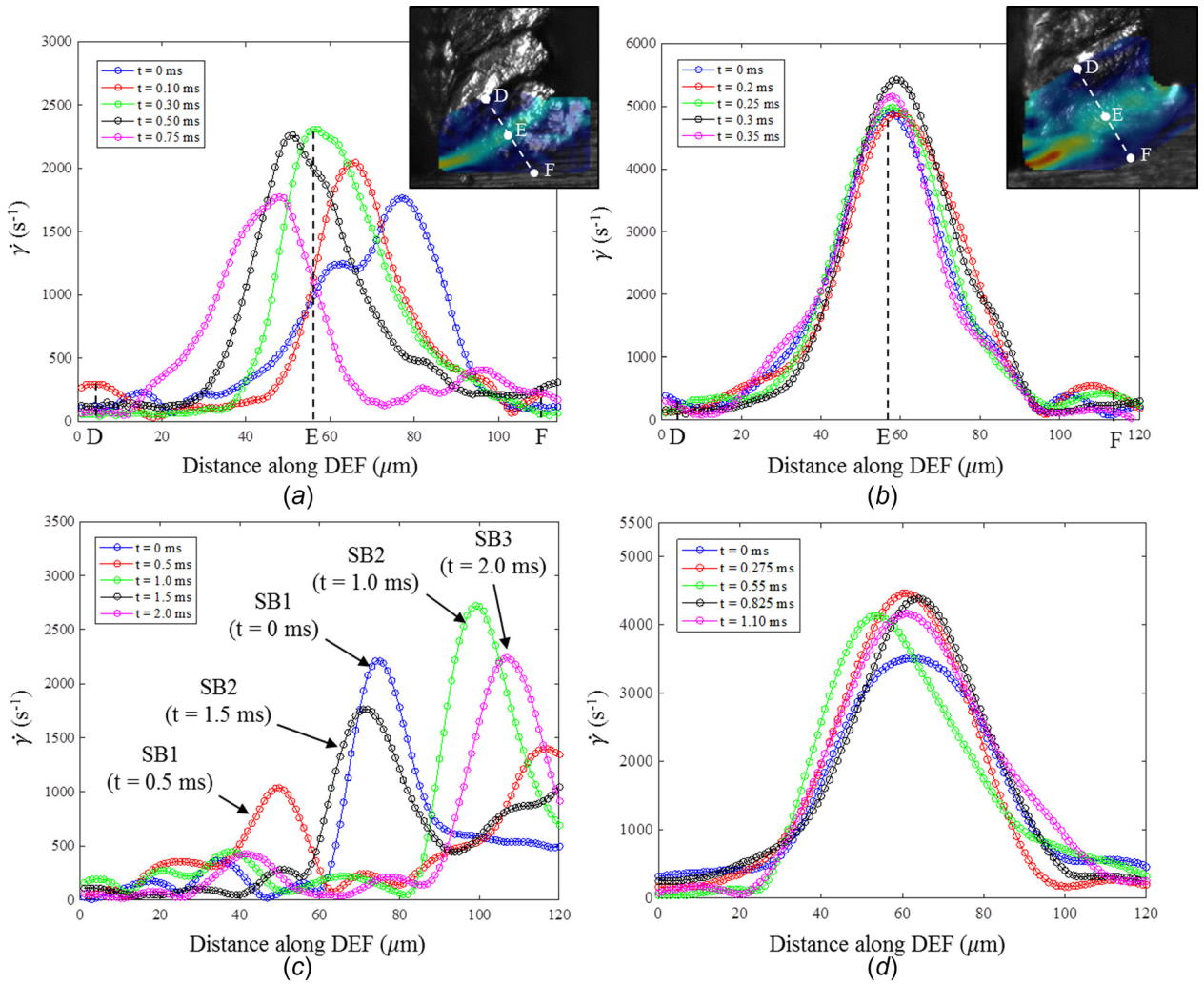

Fig. 9 Shear strain rate ($\dot{\gamma}$) progression for ECAE-processed Ti during (*a*) formation of a single saw-tooth segment (aperiodic saw-tooth chip), (*b*) formation of a single continuous chip, (*c*) formation of several aperiodic saw-tooth segments, and (*d*) formation of a single continuous chip over a longer period than in (*b*) (SB: shear band)

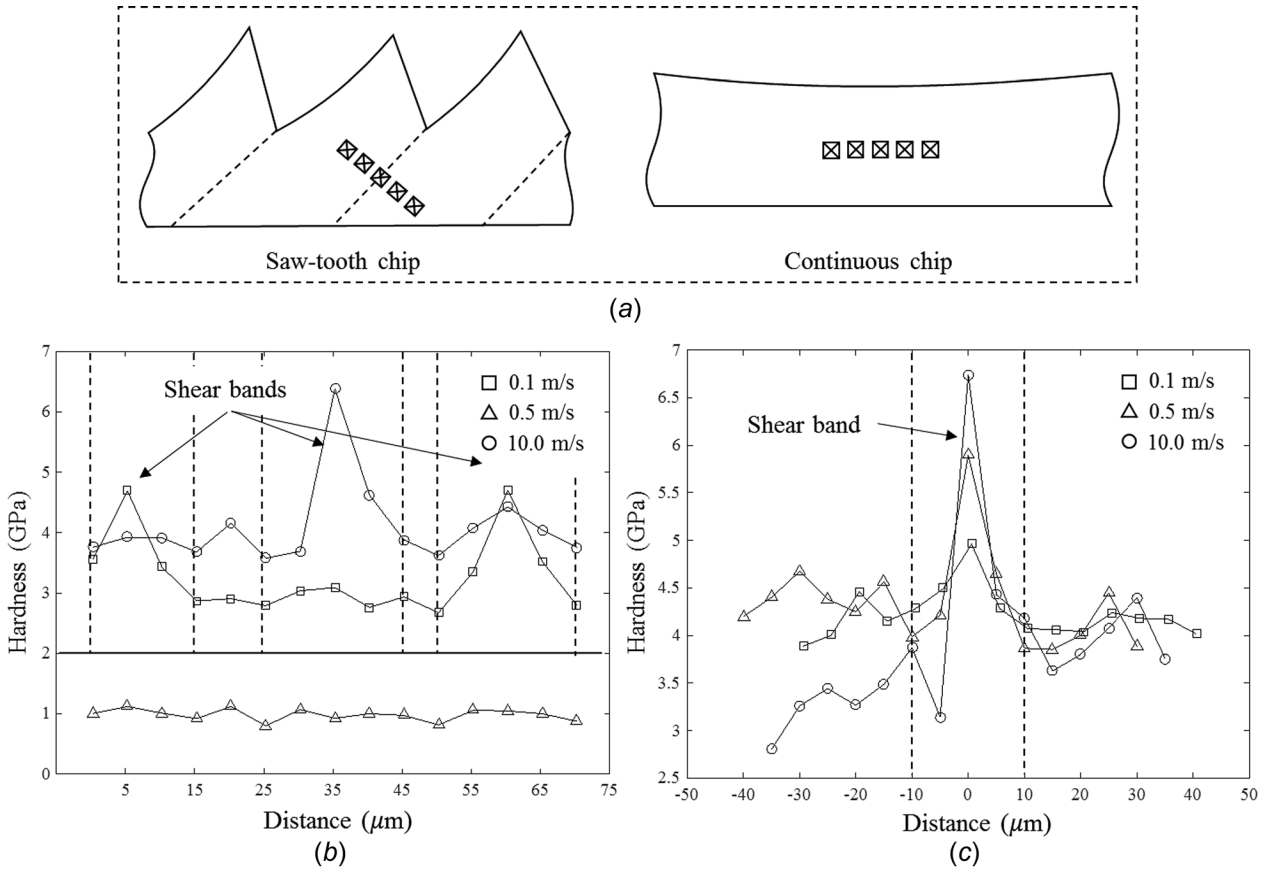

Fig. 10 Nano-indentation measurements across the PSZ: (*a*) Schematic representation of the indents for (*b*) ECAE-processed Ti and (*c*) CG Ti

et al. [34] suggested that the deformation within the bulk/interior of segments is similar to that occurring during continuous chip formation. However, in this study, the hardness found for the continuous chip morphology is much lower than that of the bulk segment of saw-tooth chips (1.0 GPa versus 3.0 – 3.8 GPa). This is most likely due to the difference in heat generated within the bulk segment of chips and the initial strain hardening during stages 1 and 2 during saw-tooth chip formation. For comparison, the hardness of CG Ti chips machined at the same cutting speeds is shown in Fig. 10(*c*). As expected, the hardness measurements are all localized within the shear bands of their saw-tooth chips, and the peak hardness value increases as the cutting speed increases. The aforesaid results show that cyclic shear localization is the governing chip formation mechanism when localized hardness peaks occur, whereas uniform shear localization is operative when the hardness is relatively constant. It is noted that the reduction in hardness due to uniform shear localization has implications for better understanding of the physical mechanism at high strain rates and elevated temperatures, and warrants further investigation in future work.

6 Conclusions

The chip morphology and chip formation mechanisms during machining of (ECAE)-processed ultrafine grained titanium (UFG Ti) have been identified using metallographic analysis together with high-speed imaging. The observations have been compared with those during machining of CG Ti, and a number of conclusions are drawn:

(1) The chip formation mechanism of the ECAE-processed Ti transitions from cyclic shear localization within the low cutting speed regime (such as 0.1 m/s or higher) to uniform shear localization within the moderately high cutting speed regime (such as $0.5 \leq V_c \leq 1.0$ m/s). When the cutting speed increases to 1.0 m/s, the chip formation mechanism transitions back to cyclic shear localization. In order to determine the specific microstructural mechanisms responsible for the changes in the chip formation mechanism, further work is required;
(2) The shear band spacing is found to increase as the cutting speed increases and is always lower than that of the CG counterpart;
(3) During machining of ECAE Ti, if the shear strain rate distribution contains a shift in the chip flow direction, the chip morphology appears saw-tooth, and cyclic shear localization is the governing chip formation mechanism. If no such shift occurs, the chip formation is considered continuous, and uniform shear localization is the governing chip formation mechanism;
(4) While the formation of pronounced shear bands is considered an indicator for the adiabatic shear localization mechanism, digital image correlation results show that shear localization may still be responsible for the formation of saw-tooth chips, regardless of the formation of pronounced shear bands. The formation of adiabatic shear bands [46] should be modeled for the understanding of the formation of saw-tooth chips; and
(5) Hardness measurements show that cyclic shear localization is the governing chip formation mechanism when localized hardness peaks occur, whereas uniform shear localization is operative when the hardness is relatively constant.

7 Future Work

To better understand the underlying physics during the ECAE-processed Ti chip formation process, much future work is

required: (1) While the DIC images produced herein provide some insight into the chip formation mechanisms, difficulties arise in identifying key features during machining, in particular, at high cutting speeds. In order to improve the quality and accuracy of the correlation, further work is required to better acquire high-speed images and delineate specific features of chip and workpiece surfaces. It should be noted that if the sliding during chip formation (stage 4) is not a continuous deformation process (that is, brittle machining instead of ductile machining), the DIC approach should not be applied to estimate shear strains and shear strain rates; (2) in this study, a zero rake angle cutting tool has been adopted to gain some machining insight during ECAE-processed Ti machining. Since cutting tools with positive rake angles are typically used to for chip flow control, the effect of rake angle on the chip morphology and chip formation mechanism should be further examined; and (3) since the dynamic material response during machining is dependent on the material microstructure, the microstructure of ECAE-processed Ti workpieces before and after machining should be carefully examined to correlate with the variation of observed chip morphologies by utilizing electron backscatter diffraction and/or transmission electron microscopy (TEM). Such microstructural changes along the chip flow direction may be further correlated with hardness measurements.

Acknowledgment

The machining support from Mr. Michael Braddock is highly appreciated.

Funding Data

- Directorate for Engineering (Grant No. 1404926).
- U.S. National Science Foundation (Grant No. NSF CMMI-1404926).

References

[1] Maleki-Ghaleh, H., Hajizadeh, K., Hadizadeh, A., Shakeri, M. S., Alamdari, S. G., Masoudfar, S., Aghaie, E., Javidi, M., Zdunek, J., and Kurzydlowski, K. J., 2014, "Electrochemical and Cellular Behavior of Ultrafine-Grained Titanium In Vitro," Mater. Sci. Eng. C, **39**, pp. 299–304.

[2] Estrin, Y., Kim, H., Lapovok, R., Ng, H., and Jo, J., 2013, "Mechanical Strength and Biocompatibility of Ultrafine-Grained Commercial Purity Titanium," BioMed. Res. Int., **2013**, pp. 1–6.

[3] Elias, C., Meyers, M., Valiev, R., and Monteiro, S., 2013, "Ultrafine Grained Titanium for Biomedical Applications: An Overview of Performance," J. Mater. Res. Technol., **2**(4), pp. 340–350.

[4] Valiev, R. Z., Islamgaliev, R. K., and Alexandrov, I. V., 2000, "Bulk Nanostructured Materials From Severe Plastic Deformation," Prog. Mater. Sci., **45**(2), pp. 103–189.

[5] Segal, V. M., 1995, "Materials Processing by Simple Shear," Mater. Sci. Eng. A, **197**(2), pp. 157–164.

[6] Zhilyaev, A., and Langdon, T., 2008, "Using High-Pressure Torsion for Metal Processing: Fundamentals and Applications," Prog. Mater. Sci., **53**(6), pp. 893–979.

[7] Sanders, P. G., Fougere, G. E., Thompson, L. J., Eastman, J. A., and Weertman, J. R., 1997, "Improvements in the Synthesis and Compaction of Nanocrystalline Materials," Nano Mater., **8**(3), pp. 243–252.

[8] Koch, C., and Cho, Y. S., 1992, "Nanocrystals by High Energy Ball Milling," Nano Mater., **1**(3), pp. 207–212.

[9] Furukawa, M., Horita, Z., Nemoto, M., and Langdon, T., 2002, "The Use of Severe Plastic Deformation for Microstructural Control," Mater. Sci. Eng. A, **324**(1–2), pp. 82–89.

[10] Barber, R. E., Dudo, T., Yasskin, P. B., and Hartwig, K. T., 2004, "Product Yield for ECAE Processing," Scr. Mater., **51**(5), pp. 373–377.

[11] Morehead, M., Huang, Y., Zhu, Y., Lowe, T., and Valiev, R., 2006, "Experimental Investigation of the Machinability of Equal Channel Angular Pressing Processed Commercially Pure Titanium," Trans. NAMRI/SME, **34**, pp. 539–546.

[12] Morehead, M., Huang, Y., and Hartwig, K. T., 2007, "Machinability of Ultrafine-Grained Copper Using Tungsten Carbide and Polycrystalline Diamond Tools," Int. J. Mach. Tools Manuf., **47**(2), pp. 286–293.

[13] Antonialli, A., Filho, A., Sordi, V., and Ferrante, M., 2012, "The Machinability of Ultrafine-Grained Grade 2 Ti Processed by Equal Channel Angular Pressing," J. Mater. Res. Technol., **1**(3), pp. 148–153.

[14] Lapovok, R., Molotnikov, A., Levin, Y., Bandaranayake, A., and Estrin, Y., 2012, "Machining of Coarse Grained and Ultra Fine Grained Titanium," J. Mater. Sci., **47**(11), pp. 4589–4594.

[15] Davis, B., Hartwig, K. T., Liang, S., and Huang, Y., 2016, "Evaluation of Chip Morphology During Machining of ECAE Titanium," International Symposium on Flexible Automation (ISFA), Cleveland, OH, Aug. 1–3, pp. 418–421.

[16] Recht, R., 1964, "Catastrophic Thermoplastic Shear," ASME J. Appl. Mech., **31**(2), pp. 189–193.

[17] Komanduri, R., and von Turkovich, B., 1981, "New Observations on the Mechanism of Chip Formation When Machining Titanium Alloys," Wear, **69**(2), pp. 179–188.

[18] Shaw, M., and Vyas, A., 1983, "Chip Formation in the Machining of Hardened Steels," CIRP Ann. Manuf. Technol., **42**(1), pp. 29–33.

[19] Shaw, M., 1980, *Metal Cutting Principles*, 2nd ed., Oxford University Press, Oxford, New York.

[20] Shankar, M., Rao, B., Lee, S., Chandrasekar, S., King, A., and Compton, W., 2006, "Severe Plastic Deformation (SPD) of Titanium at Near-Ambient Temperature," Acta Mater., **54**(14), pp. 3691–3700.

[21] Lee, S., Hwang, J., Shankar, M., Chandrasekar, S., and Compton, W., 2006, "Large Strain Deformation Field in Machining," Metall. Mater. Trans. A, **37**(5), pp. 1633–1643.

[22] Cotterell, M., and Byrne, G., 2008, "Dynamics of Chip Formation During Orthogonal Cutting of Titanium Alloy Ti-6Al-4V," CIRP Ann. Manuf. Technol., **57**(1), pp. 93–96.

[23] Pottier, T., Germain, G., Calamaz, M., Morel, A., and Coupard, D., 2014, "Sub-Millimeter Measurement of Finite Strains and Cutting Tool Tip Vicinity," Exp. Mech., **54**(6), pp. 1031–1042.

[24] Morehead, M., Huang, Y., and Luo, J., 2007, "Chip Morphology Characterization and Modeling in Machining Hardened 52100 Steels," Mach. Sci. Technol., **11**(3), pp. 335–354.

[25] Oliver, W. C., and Pharr, G. M., 2004, "Measurement of Hardness and Elastic Modulus by Instrumented Indentation: Advances in Understanding and Refinements to Methodology," J. Mater. Res., **19**(1), pp. 3–20.

[26] Barry, J., and Byrne, G., 2002, "The Mechanisms of Chip Formation in Machining Hardened Steels," ASME J. Manuf. Sci. Eng., **124**(3), pp. 528–535.

[27] Sheikh-Ahmad, J. Y., Quarless, V., and Bailey, J. A., 2004, "On the Role of Microcracks on Flow Instability in Low Speed Machining of CP Titanium," Mach. Sci. Technol., **8**(3), pp. 415–430.

[28] Davis, B., Schueller, J. K., and Huang, Y., 2015, "Study of Ionic Liquid as Effective Additive for Minimum Quantity Lubrication During Titanium Machining," Manuf. Lett., **5**, pp. 1–6.

[29] Davis, B., Liou, F., and Huang, Y., 2015, "Study of Grain Size Variation and Saw-Tooth Spacing During Machining of Additively Manufactured Titanium Alloy," MRS Commun., **5**(2), pp. 341–346.

[30] Ye, G., Chen, Y., Xue, S., and Dai, L., 2014, "Critical Cutting Speed for Onset of Serrated Chip Flow in High Speed Machining," Int. J. Mach. Tools Manuf., **86**, pp. 18–33.

[31] Molinari, A., Musquar, C., and Sutter, G., 2002, "Adiabatic Shear Banding in High Speed Machining of Ti-6Al-4V: Experiments and Modeling," Int. J. Plast., **18**(4), pp. 443–459.

[32] Chen, G., Ren, C., Yang, X., Jin, X., and Guo, T., 2011, "Finite Element Simulation of High-Speed Machining of Titanium Alloy (Ti–6Al–4V) Based on Ductile Failure Model," Int. J. Adv. Manuf. Technol., **56**(9–12), pp. 1027–1038.

[33] Yang, Q., Liu, Z., and Wang, B., 2012, "Characterization of Chip Formation During Machining 1045 Steel," Int. J. Adv. Manuf. Technol., **63**(9–12), pp. 881–886.

[34] Calamaz, M., Coupard, D., and Girot, F., 2008, "A New Material Model for 2D Numerical Simulation of Serrated Chip Formation When Machining Titanium Alloy Ti–6Al–4V," Int. J. Mach. Tools Manuf., **48**(3–4), pp. 275–288.

[35] Konmanduri, R., Schroeder, T., Hazra, J., Turkovich, B., and Flom, D., 1982, "On the Catastrophic Shear Instability in High-Speed Machining of an AISI 4340 Steel," ASME J. Eng. Ind., **104**(2), pp. 121–131.

[36] Sergueeva, A., Stolyarov, V., Valiev, R., and Mukherjee, A., 2001, "Advanced Mechanical Properties of Pure Titanium With Ultrafine Grained Structure," Scr. Mater., **45**(7), pp. 747–752.

[37] Wang, Y., Huang, J., Jiao, T., Zhu, Y., and Hamza, A., 2007, "Abnormal Strain Hardening in Nanostructured Titanium at High Strain Rates and Large Strains," J. Mater. Sci., **42**(7), pp. 1751–1756.

[38] Efe, M., Moscoso, W., Trumble, K., Compton, D., and Chandrasekar, S., 2012, "Mechanics of Large Strain Extrusion Machining and Application to Deformation Processing of Magnesium Alloys," Acta Mater., **60**(5), pp. 2031–2042.

[39] Zhang, D., Zhang, X. M., Xu, W. J., and Ding, H., 2016, "Stress Field Analysis in Orthogonal Cutting Process Using Digital Image Correlation Technique," ASME J. Manuf. Sci. Eng., **139**(3), p. 031001.

[40] Baizeau, T., Campocasso, S., Fromentin, G., and Besnard, R., 2017, "Kinematic Field Measurements During Orthogonal Cutting Tests Via DIC with Double-Frame Camera and Pulsed Laser Lighting," Exp. Mech., **57**(4), pp. 581–591.

[41] Black, J. T., 1972, "Shear Front-Lamella Structure in Large Strain Plastic Deformation Processes," ASME J. Eng. Ind., **94**(1), pp. 307–313.

[42] Gu, L., Wang, M., Chen, H., and Kang, G., 2015, "Experimental Study on the Process of Adiabatic Shear Fracture in Isolated Segment Formation in High Speed Machining of Hardened Steel," Int. J. Adv. Manuf. Technol., **86**(1–4), pp. 67–69.

[43] Gu, L., Wang, M., and Duan, C., 2013, "On Adiabatic Shear Localized Fracture During Serrated Chip Evolution in High Speed Machining of Hardened AISI 1045 Steel," Int. J. Mech. Sci., **75**, pp. 288–298.

[44] Ko, Y., Lee, C., Shin, D., and Semiatin, S., 2006, "Low-Temperature Superplasticity of Ultra-Fine-Grained Ti-6Al-4V Processed by Equal Channel Angular Pressing," Metall. Mater. Trans. A, **37**, pp. 381–391.

[45] Davis, B., 2017, "Study of the Dynamic Material Behavior and Its Correlation to the Chip Formation Mechanism and Chip Morphology During Machining," Ph.D. dissertation, University of Florida, Gainesville, FL.

[46] Zhang, X., Shivpuri, R., and Srivastava, A. K., 2016, "Chip Fracture Behavior in the High Speed Machining of Titanium Alloys," ASME J. Manuf. Sci. Eng., **138**(8), p. 081001.